Particle resolved simulation of a 3D periodic Couette dense fluid-particle flow

Oliver Scorsim, Pascal Fede, Olivier Simonin, Stéphane Vincent

Particle resolved simulation of a 3D periodic Couette dense fluid-particle flow

Oliver Scorsim[1], **Pascal Fede**[1], **Olivier Simonin**[1] **and Stephane Vincent**[2]

[1] *Institut de Mécanique des Fluides de Toulouse (IMFT)-Université de Toulouse, CNRS, INPT, UPS, FR-31400 Toulouse FRANCE*
[2] *Université Paris-Est Marne-La-Vallée (UPEM), Laboratoire MSME, Equipe TCM, Marne-La-Vallée, France*

Abstract

Dense fluid-particle flow occurs in many industrial applications, such as fluidized bed technology. To model these flows, statistical approaches are developed and, since quite recently, particle resolved simulations may be used to support the validation and the development of models. The viscous penalty method is used here to track moving solid particles coupled with the Direct Numerical Simulation (DNS) of the interstitial fluid flow. Particle-particle collisions are taken into account by Discrete Element Method (DEM) as well as the lubrication forces. 3D direct numerical simulations have been carried out of a periodic Couette flow were performed for finite Stokes number and moderate Reynolds number values for dense flows ranging from 5 to 30%. The results show a particle accumulation - at the centre or at the wall- according to the Stokes number and particle volume fraction. The production, diffusive, collisional and fluid interaction terms are analyzed for the momentum equation and particle kinetic stress equation as well.

Keywords: Direct Numerical Simulation, Fluid-Particle 3D Couette Flow, Kinetic Theory

1. Introduction

Fluid-particle flow occurs in many industrial (oil cracking, pulverized coal boiler, fluorination of uranium) and environmental areas (sediment transport, polutant dispersion). The numerical simulation of particle-laden flows has gained a lot interest since a few decades, first because it permits the study of the flow at relatively low cost and second, because it is difficult to experimentally access important parameters of such flow. Several methods exist to compute the particle-laden flows. The Euler-Euler approaches are able to perform numerical simulations at the reactor scale, but they still rely on several assumptions those can be addressed by DNS. The numerical simulations performed at the scale of the particle allow to understand the local fluid-particle interaction [4]. As such a method has a high computation cost it is then restricted to academic configurations such as Couette flow.

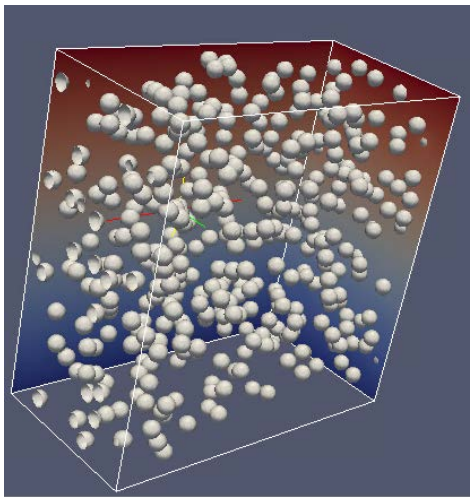

Figure 1: Instantaneous field of a fully resolved DNS with 382 particles (Case A).

2. Numerical Method

In the literature several methods can be found for performing Direct Numerical Simulation (DNS) of particle-laden flow: Lattice Boltzmann approach [2], Immersed Boundary Method [8] and Viscous Penalty Method [9]. The present numerical simulations have been carried out by using the viscous penalty method that allows to track moving solid particles coupled with the DNS of the interstitial fluid flow. Particle-particle hard-sphere collisions are taken into account by Discrete Element Method (DEM) as well as the lubrication forces [3].

Table 1: Fluid and particle material properties.

Particle diameter	d_p	$6.0\ 10^{-3}$ m
Particle density	ρ_p	$1.0\ 10^{3}$ kg/m^3
Fluid density	ρ_f	$1.0\ 10^{1}$ kg/m^3
Fluid viscosity	μ_f	$3.8\ 10^{-3}$ Pa.s
Domain dimension	H	$1.2\ 10^{-1}$ m

The computational domain is a box of length $L_x = H$, $L_y = H$, and $L_z = H/2$. In streamwise direction (x-direction) and spanwise (z-direction) periodic boundary conditions are applied. In y-direction two moving walls with no-slip boundary conditions for the fluid phase take place. For the particle, free-slip wall boundary condition is imposed.

Four cases have been considered differing by two the particle volume fraction and by the imposed wall velocity V_w. These set-up parameters are shown by Table 2. The material properties of the fluid and particle are gathered in Table 1 and the different cases in Table 2. Figure 1 shows an instantaneous field of the numerical simulation.

The mesh used is a structured grid with $N_x = N_y = 2N_z = 240$ cells in each direction. Following Vincent et al. [9] the number of cell has been chosen in order that $d_p/\Delta_x = 12$ where $\Delta_x = \Delta_y = \Delta_z = 5\ 10^{-4}$ m is the mesh size.

Table 2: Description of the cases with N_p the particle number, $\alpha_{p,bulk}$ the particle volume fraction, V_w the wall velocity, $St_{bulk} = \tau_p V_w/H$ the Stokes number and $Re_f = \rho_f V_w H/\mu_f$ the fluid Reynolds number.

CASE	N_p	$\alpha_{p,bulk}$	V_w	St_{bulk}	Re_f
A	382	5%	1.14 m/s	10	360
B	2292	30%	1.14 m/s	10	360
C	382	5%	3.42 m/s	30	1080
D	1146	15%	3.42 m/s	30	1080

3. First Results

At $t = 0$ the particles are uniformly and randomly distributed in the domain without overlapping between particles. As shown by Figure 2 the whole particle agitation reaches a steady state that for case A is approximately at 10 s.

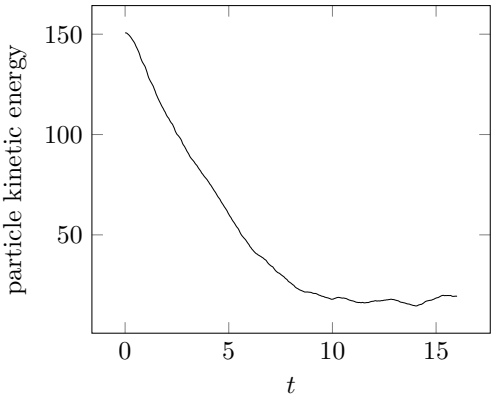

Figure 2: Total particle agitation for the case A.

The cumulative number of particles in contact, N_c, is shown by the Figure 3. One can observe at 10 s , that N_c has a linear time-evolution indicating also a steady-state. From the cumulative number of particles in contact, the collision frequency in the whole box can be computed as

$$f_c = \frac{1}{2}\frac{d}{dt}(N_c) \tag{1}$$

and the inter-particle collision timescale reads

$$\tau_c = \frac{N_p}{2f_c} \tag{2}$$

The Table 3 shows the time-average values of the inter-particle collision frequency and timescale for each case.

Table 3: Collision frequency and collision time-scale.

CASE	f_c	τ_c
A	260 col/s	0.7346 s
B	1049 col/s	1.0924 s
C	4315 col/s	0.04426 s
D	28675 col/s	0.01998 s

Interestingly, at steady-state, for the case A, all the particles tend to migrate to centre of the flow, and at the opposite, for the case C, they tend to migrate towards to the wall, that is highlighted at the Figure 4.

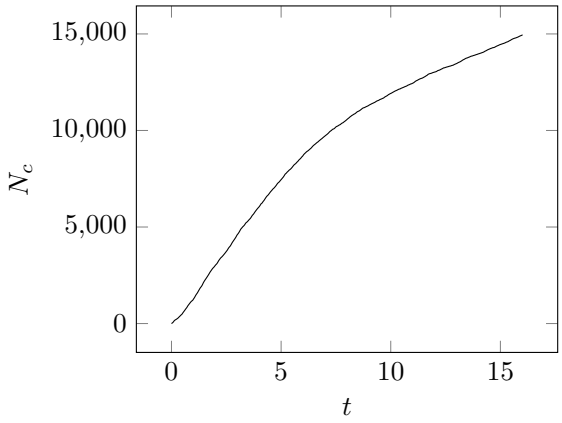

Figure 3: Cumulative number of particle in contact (N_c) for the case A.

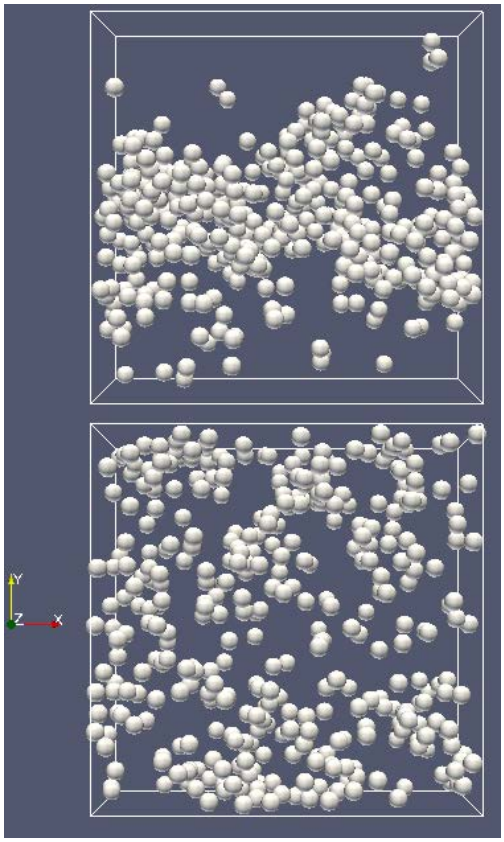

Figure 4: Effect of the wall slip velocity on the instantaneous distribution of particles at steady-state in case A (top) and case C (bottom). The particle volume fraction is $\alpha_{p,bulk} = 5\%$.

Figure 4 shows instantaneous particle distribution found at steady-state for the same solid volume fraction ($\alpha_{p,bulk} = 5\%$) but different wall velocity. On can observed that for the low velocity (case A) the particles are much more located at the centre of the domain. Large-scale clusters are also found. In contrast, for $V_w = 3.42\,\mathrm{m/s}$ the particle distribution is much more uniform across the domain.

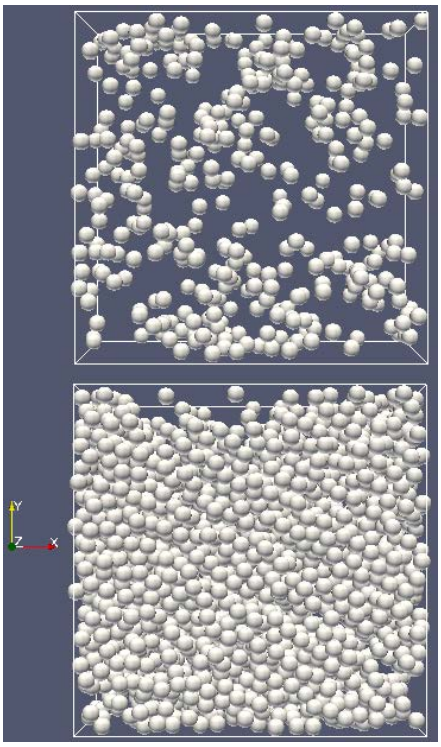

Figure 5: Effect of the particle volume fraction on the instantaneous distribution of particles at steady-state in case A (top) and case B (bottom). The wall slip velocity is $V_w = 1.14\,\mathrm{m/s}$.

Figure 5 shows the instantaneous particle distributions for the same wall velocity ($V_w = 1.14\,\mathrm{m/s}$) but different particle volume fractions. As expected, increasing the particle volume fraction leads to increase the inter-particle collisions and then the particles are much more uniformly distributed in the domain.

4. Results and discussion

The time-average variables, shown in this section, are computed at the steady-state and during a sufficiently long time in order to get converged statistics. The focus is made on the case C.

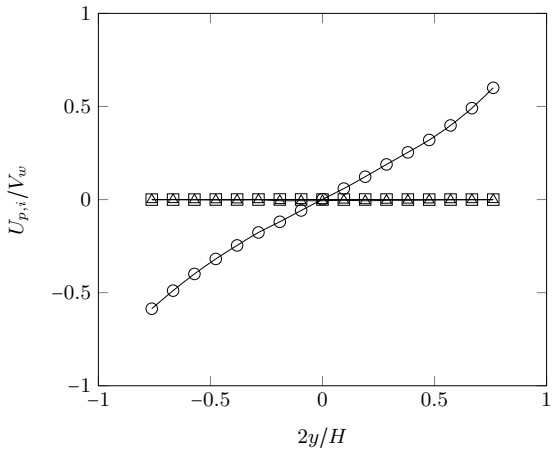

Figure 6: Mean particle velocity normalized by the wall slip velocity with respect to the wall-distance. The symbols are —○—: $U_{p,x}/V_w$; —□—: $U_{p,y}/V_w$; —△—: $U_{p,z}/V_w$

The mean particle velocities are shown by Figure 6. Wall-normal and spanwise mean particle velocities are equal to zero. In contrast the streamwise particle velocity exhibit a linear shear in the core of the flow.

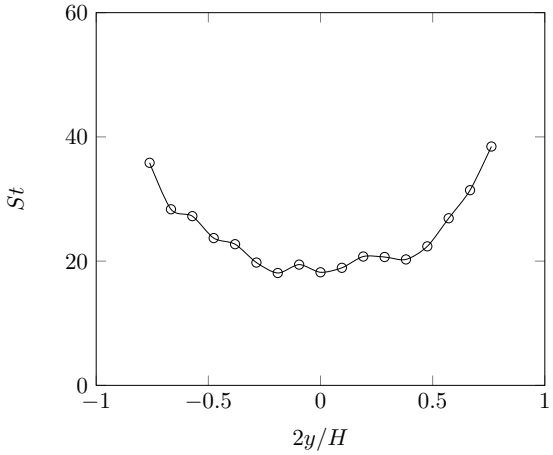

Figure 7: Stokes number with respect to the wall-distance.

Figure 7 shows the Stokes number profile. It is defined as $St = \tau_p\,\partial U_{p,x}/\partial y$ where the particle response time is given by $\tau_p = \rho_p d_p^2/18\mu_f$. At the centre of the domain the Stokes number profile is about 20 and increases close to the two moving wall. As τ_p is given constant, the evolution of the Stokes number is coming from change of the velocity shear across the channel which, in this case, is roughly constant for $2y/H$ between -0.3 and +0.3.

As shown by Figure 8 the wall-normal distribution of the particles across the domain is not uniform. The particles are more present in the near wall region and less in the core of the domain.

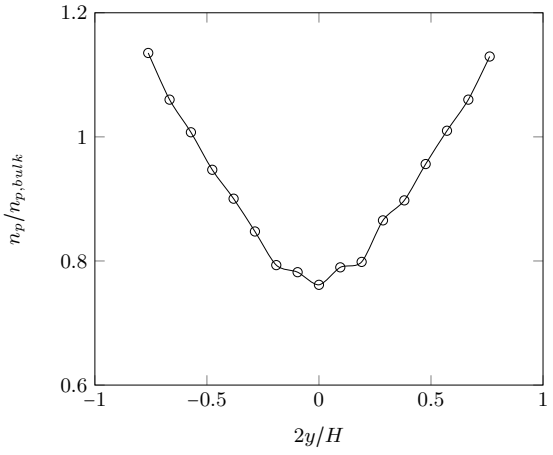

Figure 8: Particle number density with respect to the wall-distance.

The particle kinetic stress tensor is defined by $R_{p,ij} = \langle u'_{p,i}u'_{p,j}\rangle_p$ where $u'_{p,i}$ is the particle velocity fluctuation. Figure 10 shows all components of the particle kinetic stress tensor with respect to the distance with the wall. It shows that the particle agitation in strongly anisotropic and is measured essentially in the streamwise direction. The spanwise and the wall-normal particle kinetic stress component are nearly the same. In addition $R_{p,xz}$ and $R_{p,yz}$ are found close to zero. As expected the shear component, $R_{p,xy}$, is negative.

The particle kinetic agitation corresponds to the trace of the particle kinetic stress tensor. Then it is defined by $q_p^2 = 1/2R_{p,ii}$.

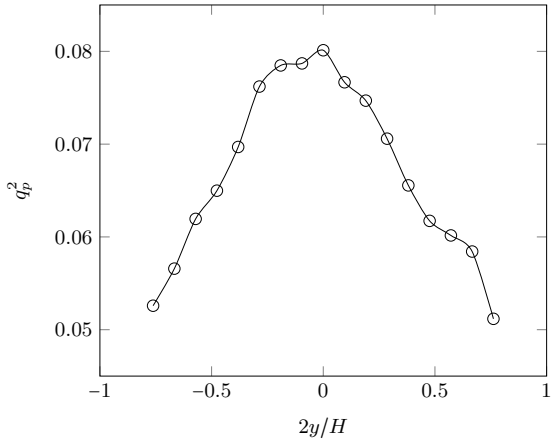

Figure 9: Particle kinetic agitation q_p^2 with respect to the wall-distance.

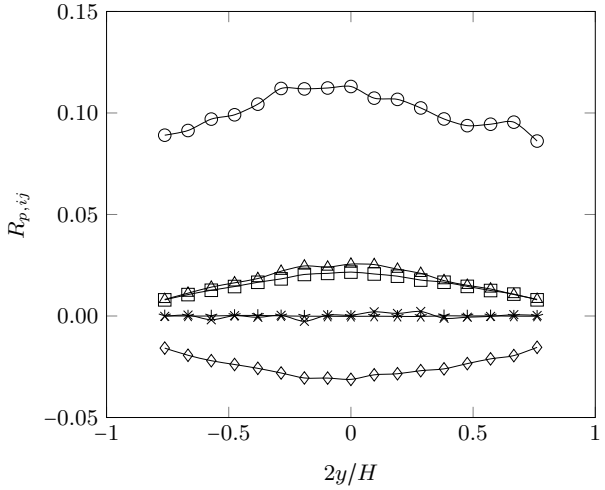

Figure 10: Particle kinetic stress tensor $R_{p,ij}$ with respect to the wall-distance. The symbols are —○—: $R_{p,xx}$; —□—: $R_{p,yy}$; —△—: $R_{p,zz}$; —◇—: $R_{p,xy}$; —×—: $R_{p,xz}$ and —✶—: $R_{p,yz}$

The profile of q_p^2 is shown by Figure 9. One can notice that the agitation of the particles is higher at the centre of the domain, where particle volume fraction is lower.

In the framework of a statistical description of granular flow [7] the transport equation of each moment of the particulate phase can be derived. By assuming that $U_{p,y}$, $U_{p,z}$ and the gradient in x- and z-direction are negligibles , momentum equation writes

$$\frac{\partial U_{p,i}}{\partial t} = -\frac{1}{n_p}\frac{\partial\left(n_p R_{p,iy}\right)}{\partial y} + \langle a_i^f \rangle_p + \frac{1}{n_p}\mathbb{C}\left(u_{p,i}\right) \tag{3}$$

where $\langle a_i^f \rangle_p$ is the acceleration of the particles due to fluid interaction.

Budget balance of Eq. (3), in the y- direction, is shown by Figure 11. One can notice that a balance is established between the production term, which tends to move the particles towards the walls and and the fluid interaction term which leads the particles towards the centre.

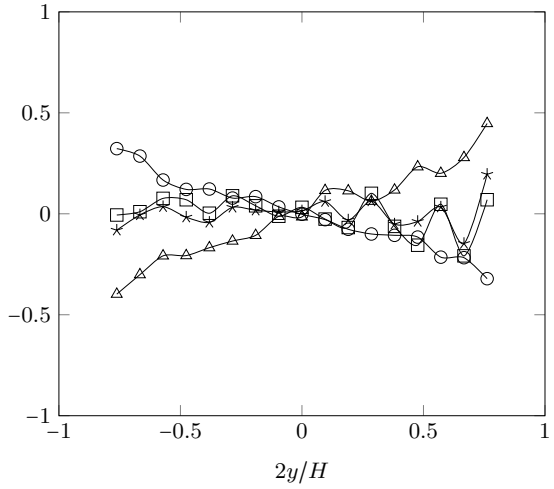

Figure 11: Budget analysis of the transport equation of $U_{p,y}$ given by Eq. (3). The symbols are —△—: $-1/n_p\partial\left(n_p R_{p,yy}\right)/\partial y$; —○—: $\langle a_y \rangle_p$; —□—: $\mathbb{C}\left(u_{p,i}\right)/n_p$; —✶—: sum of all terms.

The particle kinetic tensor transport equation can also be derived. With the same assumptions, the equations for $R_{p,xx}$, $R_{p,yy}$, $R_{p,zz}$,$R_{p,xy}$ and q_p^2 read

$$\begin{aligned}\frac{\partial R_{p,xx}}{\partial t} &= -\frac{1}{n_p}\frac{\partial\left(n_p S_{p,yxx}\right)}{\partial y} - 2R_{xy}\frac{\partial U_{p,x}}{\partial y} \\ &+ 2\langle a_x^f u'_{p,x}\rangle_p + \frac{1}{n_p}\mathbb{C}\left(u'_{p,x}u'_{p,x}\right)\end{aligned} \tag{4}$$

$$\begin{aligned}\frac{\partial R_{p,yy}}{\partial t} &= -\frac{1}{n_p}\frac{\partial\left(n_p S_{p,yyy}\right)}{\partial y} \\ &+ 2\langle a_y^f u'_{p,y}\rangle_p + \frac{1}{n_p}\mathbb{C}\left(u'_{p,y}u'_{p,y}\right)\end{aligned} \tag{5}$$

$$\begin{aligned}\frac{\partial R_{p,zz}}{\partial t} &= -\frac{1}{n_p}\frac{\partial\left(n_p S_{p,yzz}\right)}{\partial y} \\ &+ 2\langle a_z^f u'_{p,z}\rangle_p + \frac{1}{n_p}\mathbb{C}\left(u'_{p,z}u'_{p,z}\right)\end{aligned} \tag{6}$$

$$\begin{aligned}\frac{\partial R_{p,xy}}{\partial t} &= -\frac{1}{n_p}\frac{\partial\left(n_p S_{p,xyy}\right)}{\partial y} - R_{p,yy}\frac{\partial U_{p,x}}{\partial y} \\ &+ \langle a_x^f u'_{p,y}\rangle + \langle a_y^f u'_{p,x}\rangle_p + \frac{1}{n_p}\mathbb{C}\left(u'_{p,x}u'_{p,y}\right)\end{aligned} \tag{7}$$

$$\begin{aligned}\frac{\partial q_p^2}{\partial t} &= -\frac{1}{2n_p}\frac{\partial\left(n_p S_{p,yii}\right)}{\partial y} - R_{xy}\frac{\partial U_{p,x}}{\partial y} \\ &+ \langle a_i^f u'_{p,i}\rangle + \frac{1}{n_p}\mathbb{C}\left(u'_{p,i}u'_{p,i}\right)\end{aligned} \tag{8}$$

In Eqs. (4)-(8), $S_{p,ijk} = \langle u'_{p,i}u'_{p,j}u'_{p,k}\rangle$ is the third order correlation of the particle fluctuating velocity. Figure 12 - 15 shows each contribution of Eq. (4) - Eq. (7). One can observe that in x-direction the particle kinetic stress is produced by the mean shear. As expected the friction of the particles with the fluid leads to the destruction of the particle kinetic stress component $R_{p,xx}$, $R_{p,yy}$, $R_{p,zz}$ and $R_{p,xy}$. In the x- and z- direction the inter-particle interactions is negative meaning that the collisions decrease the particle kinetic stress component. In contrast in y-direction the inter-particle interaction term is positive meaning that the collisions increase $R_{p,yy}$ and $R_{p,zz}$. This effect is due to the nature of the collisions that is an isotropization effect. In the present case, the particle agitation in x-direction is redistributed towards y- and z-direction by the inter-particle collision [10]. Such kind of behavior has also been found at [11, 12].

A diffusive term is also found near the centre of the domain for the budgets of $R_{p,xx}$, $R_{p,yy}$ and $R_{p,xy}$, this effect leads to the transport of agitation away of the centre.

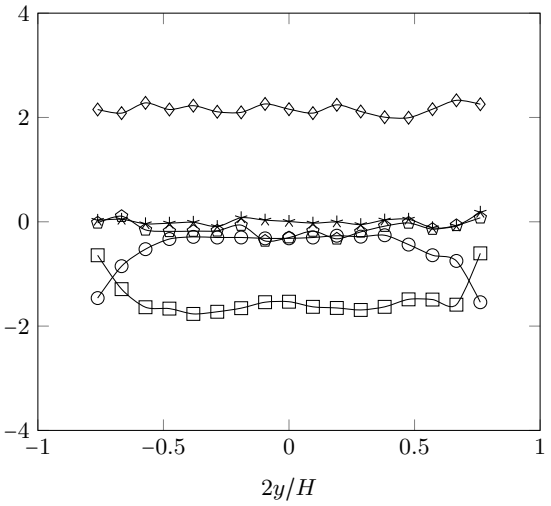

Figure 12: Budget analysis of the transport equation of $R_{p,xx}$ given by Eq. (4). The symbols are —◇—: $-1/n_p\partial\left(n_p S_{p,yxx}\right)/\partial y$; —◇—: $-2R_{xy}\partial U_{p,x}/\partial y$; —○—: $2\langle a_x^f u'_{p,x}\rangle_p$; —□—: $\mathbb{C}\left(u'_{p,x}u'_{p,x}\right)/n_p$; —⋆—: sum of all the terms.

The terms of the evolution of the particle agitation equation given by Eq. (8) are depicted by Figure 16. One can notice that the global effect is that the random kinetic energy is produced by the mean particle shear velocity, and it is dissipated by the collisions and the interaction with the fluid.

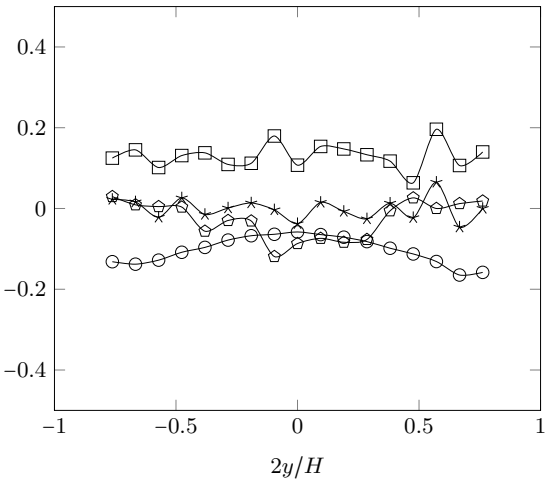

Figure 13: Budget analysis of the transport equation of $R_{p,yy}$ given by Eq. (5). The symbols are —◇—: $-1/n_p\partial\left(n_p S_{p,yyy}\right)/\partial y$; —○—: $2\langle a_y^f u'_{p,y}\rangle_p$; —□—: $\mathbb{C}\left(u'_{p,y}u'_{p,y}\right)/n_p$; —⋆—: sum of all terms.

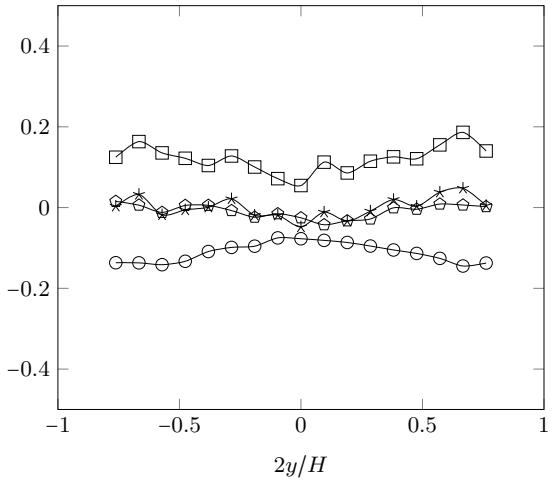

Figure 14: Budget analysis of the transport equation of $R_{p,zz}$ given by Eq. (6). The symbols are —◇—: $-1/n_p\partial\left(n_p S_{p,yzz}\right)/\partial y$; —○—: $2\langle a_z^f u'_{p,z}\rangle_p$; —□—: $\mathbb{C}\left(u'_{p,z}u'_{p,z}\right)/n_p$; —⋆—: sum of all terms.

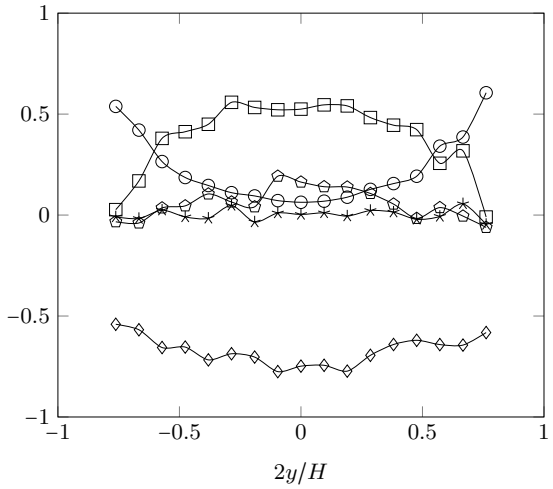

Figure 15: Budget analysis of the transport equation of $R_{p,xy}$ given by Eq. (7). The symbols are —◇—: $-1/n_p\partial\left(n_p S_{p,xyy}\right)/\partial y$; —◇—: $-R_{p,yy}\partial U_{p,x}/\partial y$; —○—: $\langle a_x^f u'_{p,y}\rangle + \langle a_y^f u'_{p,x}\rangle_p$; —□—: $\mathbb{C}\left(u'_{p,x}u'_{p,y}\right)/n_p$; —⋆—: sum of all terms.

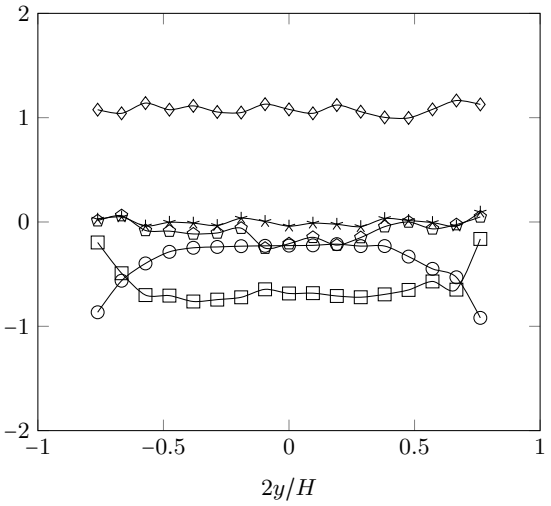

Figure 16: Budget analysis of the transport equation of q_p^2 given by Eq. (8). The symbols are —○—: $-1/(2n_p)\,\partial\left(n_p S_{p,ykk}\right)/\partial y$; —◇—: $-R_{xy}\partial U_{p,x}/\partial y$; —○—: $\langle a_k^f u'_{p,k}\rangle_p$; —□—: $\mathbb{C}\left(u'_{p,k}u'_{p,k}\right)/(2n_p)$; —✶—: sum of all terms.

5. Conclusion

3D dense fluid-particle Couette flow were studied using direct numerical simulation. Fundamental parameters of the flow have been extracted from the steady-state such as, particle kinetic stress tensor, third order correlation, collision time-scale, etc. The production, diffusion, collisional and fluid interaction terms were analyzed highlighting fundamental physics of the flow, such as the isotropization effect with the collisions.

6. Acknowledgments

The authors acknowledge the support from the Brazilian funding agency CAPES (Science-Without-Borders - scholarship: 13172-13-1). This work was granted access to the HPC resources of CALMIP supercomputing center under the allocation 2015-[p0111] and 2016-[p1529].

References

[1] S. Chapman, T. G. Cowling, The mathematical theory of non-uniform gases: an account of the kinetic theory of viscosity, thermal conduction and diffusion in gases. *Cambridge university press.*, 1970.

[2] A.T. Cate, J.J. Derksen, L.M. Portela, H.E.A. Van Den Akker, Fully resolved simulations of colliding monodisperse spheres in forced isotropic turbulence. *Journal of Fluid Mechanics*, 519, 2004.

[3] J.C. Brändle de Motta, W.-P. Breugem, B. Gazanion, J.-L. Estivalèzes, S. Vincent, E. Climent, Numerical modelling of finite-size particle collision in a viscous fluid. *Phys. Fluids*, 25, 083302, 2013.

[4] J.C. Brändle de Motta, Simulation des ecoulements turbulents avec des particules de taille finie en regime dense. *PhD Thesis*, Institut Supérieur de l'Aeronautique et de l'Espace (ISAE), 2013.

[5] T.N. Randrianarivelo, Etude numérique des interactions hydrodynamiques fluides/solides: application aux lits fluidisés. *PhD thesis*, Bordeaux 1, 2005.

[6] A.J. Sarthou, Méthodes de domaines fictifs d'ordre élevé pour les équations elliptiques et de Navier-Stokes: application au couplage fluide-structure. *PhD thesis*, Bordeaux 1, 2009.

[7] O. Simonin, Continuum modelling of dispersed two-phase flows. Lecture Series 1996-02, von Karman Institute for Fluid Dynamics, K1-K47, 1996.

[8] M. Uhlmann, An immersed boundary method with direct forcing for the simulation of particulate flows. *Journal of Computational Physics*, 448 - 476, 209, 2005.

[9] S. Vincent, J.C. Brändle de Motta, A. Sarthou, J.-L. Estivalèzes, O. Simonin, E. Climent, A Lagrangian VOF tensorial penalty method for the DNS of resolved particle-laden flows. *Journal of Computational Physics*, vol. 256, pp. 582-614, 2014

[10] N. Caraman, J. Borée, and O. Simonin. Effect of collisions on the dispersed phase fluctuation in a dilute tube flow: Experimental and theoretical analysis. *Physics of Fluids*, 15.12: 3602-3612, 2003

[11] J. F. Parmentier, O. Simonin. Transition models from the quenched to ignited states for flows of inertial particles suspended in a simple sheared viscous fluid. *Journal of Fluid Mechanics*, 711, 147-160, 2012.

[12] A. Boëlle, G. Balzer, O. Simonin. Second-order prediction of the particle-phase stress tensor of inelastic spheres in simple shear dense suspensions. *ASME-PUBLICATIONS-FED*, 228, 9-18, 1995